

[©2021 IEEE](#). Personal use of this material is permitted. Permission from IEEE must be obtained for all other uses, in any current or future media, including reprinting/republishing this material for advertising or promotional purposes, creating new collective works, for resale or redistribution to servers or lists, or reuse of any copyrighted component of this work in other works.

Digital Object Identifier [10.1109/TCPMT.2021.3116220](#)

IEEE Transactions on Components, Packaging and Manufacturing Technology

3-D-Printing and High-Precision Milling of W-Band Filter Components With Admittance Inverter Sequences

Chad Bartlett

Jens Bornemann

Michael Höft

Suggested Citation

C. Bartlett, J. Bornemann and M. Höft, "3-D-Printing and High-Precision Milling of W-Band Filter Components With Admittance Inverter Sequences," in *IEEE Transactions on Components, Packaging and Manufacturing Technology*, vol. 11, no. 12, pp. 2140-2147, Dec. 2021.

3D-Printing and High-Precision Milling of W-Band Filter Components with Admittance Inverter Sequences

Chad Bartlett, *Student Member, IEEE*, Jens Bornemann, *Life Fellow, IEEE*
and Michael Höft, *Senior Member, IEEE*

Abstract—This work presents the design of an additively manufactured W-band bandpass filter and a subtractively manufactured W-band diplexer in order to demonstrate the use of admittance inverter sequences for the ease of manufacture at millimetre-wave frequencies. Contrary to typical impedance inverters (E-plane and H-plane irises), the use of admittance inverters (E-plane and H-plane stubs) allow for larger dimensions to be specified and ultimately do not impede the general waveguide path. The proposed bandpass filter is designed with all E-plane stubs, while the diplexer is designed with one branch utilizing both E-plane and H-plane stubs as an arbitrary sequence, and the second branch utilizing all H-plane irises. The additively manufactured bandpass filter is fabricated using the most elementary level stereolithography (SLA) based methods, demonstrating that a hobbyist-type SLA printer and metalization method can procure exceptional results for millimeter-wave filter designs. The subtractively manufactured diplexer is fabricated using high-precision computer numerical control (CNC) milling in order to highlight the use of arbitrary inverter sequences in a more complex and robust design profile, while the dispersive transmission zeros that are caused by over-moding of the inverter stubs is utilized to demonstrate unique isolation characteristics in the upper W-band region. The design concepts, fabrication profiles, simulations and measurements which are presented in this work highlight a viable option for overcoming miniaturized dimensions in millimetre and sub-millimetre-wave applications.

Index Terms—Diplexer, fabrication techniques, filter, millimetre-wave, passive components, stereolithography, waveguide inverters, W-band, WR-10

I. INTRODUCTION

FUTURE demands for high-data rate communication systems and constellation micro-satellite networks has triggered an increasing amount of research towards overcoming the challenges of space- and sub-orbital based systems. As the electromagnetic spectrum becomes increasingly overcrowded

within the lower-frequency bands, use of the millimetre-wave frequency range offers many advantages that can be applied to the next generations of communication, radar, and satellite equipment. These advantages can be viewed not only as reductions in size and weight, but also as methods to reduce interference and harness regions with selective atmospheric attenuation [1], [2]. However, the development of components within the millimetre-wave region pose their own inherent challenges such as fabrication accuracy, surface roughness and suitable design procedures for additive manufacturing. In regards to W-band cavity-based waveguide filter designs, alternative approaches to computer numerical control (CNC) milling have been proposed throughout the literature and have been able to demonstrate a varying degree of measured results. Some of the most recent developments with regards to reported W-band results using additive manufacturing techniques include stereolithography (SLA) [3]–[5], selective laser melting (SLM) [6], selective laser sintering (SLS) [7], and micro-laser sintering (MLS) [8], [9]. In general, each of these techniques approach overcoming high-frequency fabrication challenges from a technological standpoint rather than from a circuit synthesis approach.

In [10], direct-coupled rectangular waveguide filters with arbitrary inverter sequences were proposed and many new configurations were demonstrated in the Ku-band by simulation. Although half-wave and quarter-wave techniques are well known, the use of alternating impedance and admittance inverters or all-admittance inverters are still vastly unexplored in the current literature on cavity-based waveguide components. To the authors' knowledge, only simulations proposed in [10] have been applied to demonstrate all-admittance inverter sequences in rectangular waveguide bandpass filter designs. Given that the general structure of admittance inverters are larger than their impedance inverter counterparts, their use in millimetre wave and sub-millimetre wave designs should be investigated for overcoming fabrication challenges in regards to aspect ratio, etching inconsistencies and general dimensions that are difficult to obtain. In fact, both additive and subtractive fabrication methods can greatly benefit from the alternative design profiles offered from this method; for example, thin-walled irises and narrow iris gaps which are subject to warping, under-etching or infeasible milling dimensions can be avoided all together.

Manuscript received XX XX, 2021; Revised XX XX, 2021; Accepted XX XX, 2021. This project has received funding from the European Union's Horizon 2020 research and innovation programme under the Marie Skłodowska-Curie grant agreement 811232-H2020-MSCA-ITN-2018.

C. Bartlett and M. Höft are with the Department of Electrical and Information Engineering, University of Kiel, Kiel 24118, Germany (e-mail: chb@tf.uni-kiel.de; mh@tf.uni-kiel.de).

J. Bornemann is with the Department of Electrical and Computer Engineering, University of Victoria, Victoria, BC V8W 2Y2, Canada (e-mail: j.bornemann@ieee.org). Color versions of one or more of the figures in this article are available online at <http://ieeexplore.ieee.org>.

Digital Object Identifier XXX/TMTT.XXXX

In order to further this line of research, we investigate this method as a means of overcoming difficulties with miniature filter fabrication. The designs which follow are the first examples of waveguide-based filters and duplexers that utilize inverter sequences to ease the stringent dimensions required in millimetre-wave designs. In this manner, the key underlying theme of this investigation is the utilization of inductive and capacitive stubs, where inherently, the size of the component's coupling inverters are sacrificed as a means of constructing a filter path without impeding (or interceding) the fundamental waveguide dimensions (2.54 mm x 1.27 mm for a standard WR-10 waveguide). Two inherently different methods of production are used for prototype fabrication, namely, the filter is demonstrated in SLA 3D-printing as an additively manufactured option, and the duplexer is demonstrated using high-precision CNC milling as a subtractively manufactured option. The former method that is used in this study demonstrates a very low-cost option in which a hobbyist-type SLA printer and an elementary copper-based metallization method is used for the fabrication of an all-admittance inverter (E-plane stub) filter. This SLA version of the filter is designed for a passband between 95 GHz and 105 GHz, and ultimately demonstrates that a very coarse method of fabrication can easily reach the millimetre-wave frequency range without the need of a commercial-grade SLA printer, (Ni) nickel or (Ag) silver based plating methods, or the design of complicated slot-structures to allow for internal metallization. The latter method demonstrates the use of high-precision CNC milling in order to facilitate a more complex and robust mixed-inverter duplexer structure, where the first branch of the duplexer takes the form of an all-admittance inverter filter (E-plane and H-plane stubs), and the second branch of the duplexer takes the form of an all-impedance inverter filter (H-plane irises). The admittance inverter branch is selected as the duplexer's lower passband to utilize the transmission zeros that are caused by over-moding in the upper region of the W-band. Both of the duplexer's passbands are selected for 5 GHz operation, which are designated for the ranges of 95 GHz to 100 GHz and 103 GHz to 108 GHz. Each of the components in this work exhibit passband characteristics in the upper portion of the W-band and both of the experimental prototypes are fabricated with an E-plane cut as split-block designs. A discussion on both of the design's capabilities are presented and a comparison of the simulated and measured results are discussed in order to highlight the fabrication and operational characteristics.

II. DESIGN METHODOLOGY

As part of any general synthesis procedure, the inverter type and sequence must be selected in order to facilitate the interconnection between resonator cavities. Fig. 1 depicts four of the basic waveguide inverter forms; Fig. 1(a) and 1(b) represent H-plane and E-plane admittance inverter stubs, respectively, while Fig. 1(c) and 1(d) represent H-plane and E-plane impedance inverter irises, respectively. From these representations, it is clear that the admittance inverter stubs shown in Fig. 1(a) and 1(b) will intrinsically occupy a volume

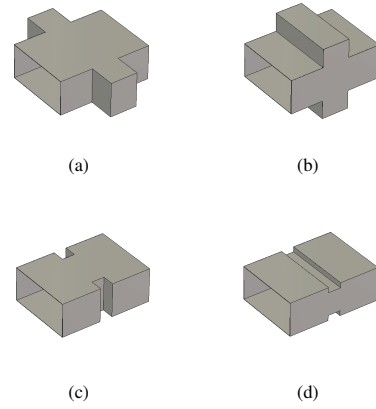


Fig. 1. Basic forms of waveguide inverters a). Inductive Stub, b). Capacitive Stub, c). Inductive Iris, and d). Capacitive Iris.

that is outside of the general waveguide dimensions. This in turn has several disadvantages; one being that the overall design becomes less compact, and the second being that over-moding can generate many spurious modes in the rejection-band regions when directly compared to impedance inverter designs [10]. However, in the case of very high-frequency designs, it may be advantageous for designers to utilize the larger and less restrictive dimensions for overcoming critical or difficult fabrication schemes, especially in the case of additive manufacturing or silicon micro-machining. The following demonstrates two examples which utilize admittance inverters for W-band operation, and use two distinctly different technologies for their inception. For both of the designs, the full-wave edge-condition-based coupled-integral-equations technique (CIET) presented in [11]–[14] and further demonstrated in [10] is used to quickly synthesize and preemptively optimize the dimensions of the proposed filter and each of the filtering branches of the duplexer before final optimization in CST Microwave Studio. As part of the final optimization, fabrication considerations are made for E-plane manufacture and the corner radii are taken into account for accurate component profiles. As follows, Section II.A outlines the all-admittance inverter filter for fabrication with a low-cost SLA-printing method, Section II.B outlines the mixed-inverter duplexer for fabrication using high-precision CNC milling, Section III presents a discussion on the fabrication routine and the measured results, Section IV compares the measured results to the state-of-the-art, and Section V serves as a conclusion.

A. 3D-Printed Admittance Inverter Filter

For the design of the filter structure, an all-admittance inverter scheme was selected as the method to demonstrate a simple and low-cost method of 3D-printing at millimetre-wave frequencies. The design procedure starts by obtaining the general Chebychev coefficients from [15] and determining the normalized inverter values with equation (1) for the admittance inverter schemes shown in Fig. 2. Equation (2) is applied in

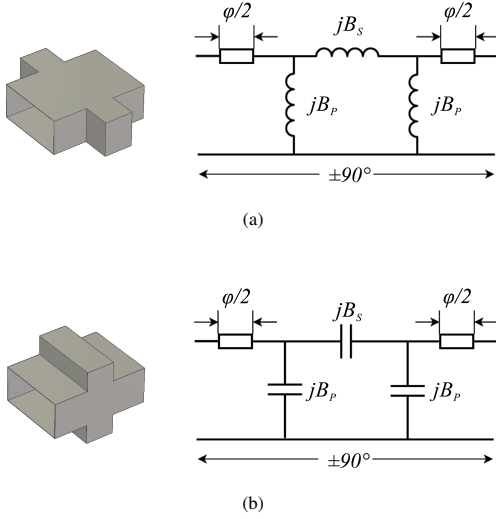


Fig. 2. Waveguide admittance inverters and their corresponding circuit topologies. (a) Inductive stub, and (b) Capacitive stub.

$$jB_p = \frac{(1 - S_{21})^2 - S_{11}^2}{(1 + S_{11})^2 - S_{21}^2} \quad (1a)$$

$$jB_s = \frac{2S_{21}}{(1 + S_{11})^2 - S_{21}^2} \quad (1b)$$

$$\phi = -\tan^{-1}(2B_s + B_p) - \tan^{-1}B_p \quad (1c)$$

$$J = \left| \tan\left(\frac{\phi}{2} + \tan^{-1}B_p\right) \right| \quad (1d)$$

$$l_i = \frac{\lambda_{go}}{2\pi} \left[\pi + \frac{1}{2}(\phi_{2,i} + \phi_{1,i+1}) \right] \quad (2)$$

order to adjust the individual resonator lengths between the selected inverters [10].

For the case at hand, the filter is designed using capacitive stubs (as shown in Fig. 2(b)) in order to achieve a passband over the 95 GHz to 105 GHz region. Synthesis based on the CIET is used for the initial design parameters, where the inverter aperture is varied in a search algorithm and the stub thickness is held constant [10], [14]. In this manner, the initial design can be quickly synthesized before a final optimization in CST Microwave Studio. Fig. 3 depicts a perspective view of the admittance inverter filter's vacuum shell and its corresponding dimensions. Fig. 4 exhibits the final simulated S-parameters of the structure depicted in Fig. 3 over the range of 85 GHz to 115 GHz. Common to stub-inverter designs, the lower rejection-band region has lower selectivity than the upper rejection-band region. This lower selectivity can be overcome by using more complex inverter sequences such as demonstrated in [10], [16]–[18], but for experimental purposes with hobbyist-type SLA printing, we resolve to first demonstrate the elementary (all-admittance inverter) configuration. The wide-band spurious performance

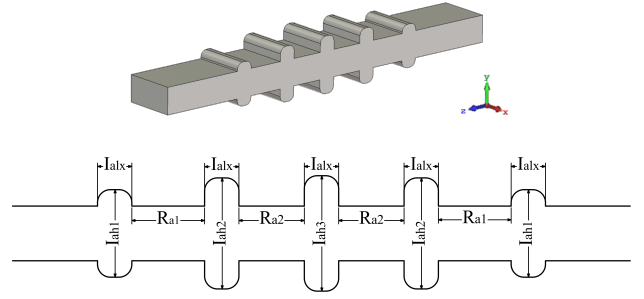


Fig. 3. Perspective view of the admittance-inverter filter's vacuum shell and its corresponding dimensions; $R_{a1} = 1.695$ mm, $R_{a2} = 1.524$ mm, $I_{alx} = 0.800$ mm, $I_{ah1} = 2.032$ mm, $I_{ah2} = 2.578$ mm, and $I_{ah3} = 2.680$ mm.

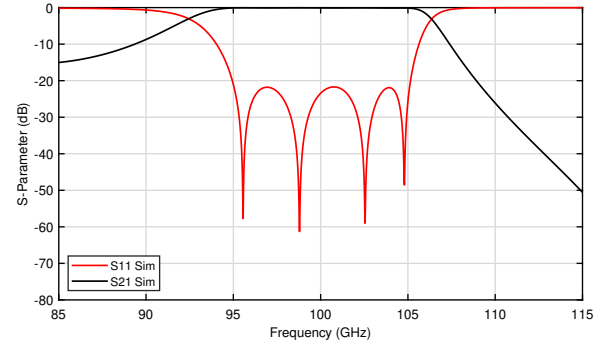


Fig. 4. S-parameters of the simulated admittance-inverter filter (conductivity of copper taken as 5.8×10^7 S/m).

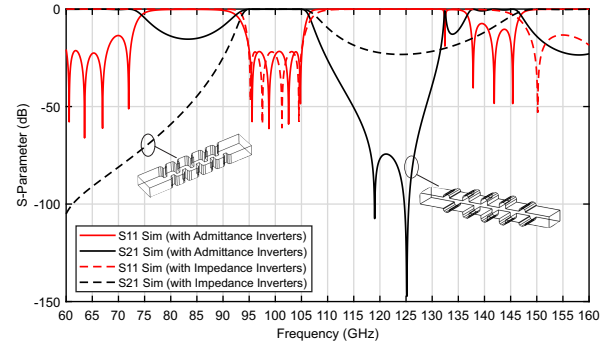


Fig. 5. Wide-band spurious performance of the simulated admittance-inverter filter with comparison to an impedance-inverter filter with similar specifications (conductivity of copper taken as 5.8×10^7 S/m).

of the filter is detailed in Fig. 5 over the range of 60 GHz to 160 GHz, where in addition, the simulated results are compared to the response of a typical fourth-order impedance inverter (all-inductive iris) filter with similar specifications. The wider range is beyond the definition of the W-band, which is 75 GHz to 110 GHz. One should be aware, that the TE_{20} mode cutoff frequency is at approximately 118 GHz, and therefore, note that slight geometrical asymmetries may excite further modes.

In regards to the proposed admittance-inverter filter design outlined in Fig. 3, a 0.3 mm radius is selected for the inner corners of the inverter stubs, however, it can be noted that the

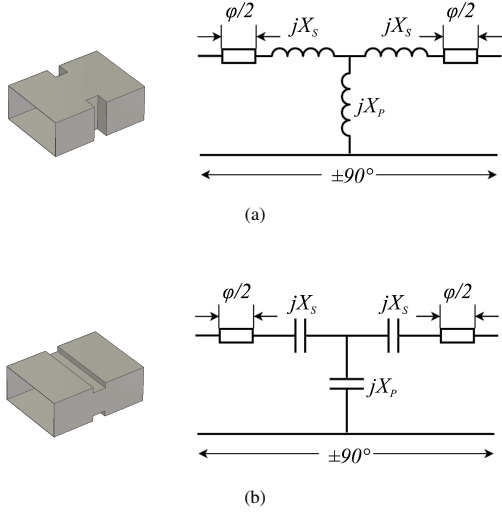


Fig. 6. Waveguide impedance inverters and their corresponding circuit topologies. (a) Inductive iris, and (b) Capacitive iris.

$$jX_s = \frac{(1 - S_{21})^2 - S_{11}^2}{(1 - S_{11})^2 - S_{21}^2} \quad (3a)$$

$$jX_p = \frac{2S_{21}}{(1 - S_{11})^2 - S_{21}^2} \quad (3b)$$

$$\phi = -\tan^{-1}(2X_p + X_s) - \tan^{-1}X_s \quad (3c)$$

$$K = \left| \tan\left(\frac{\phi}{2} + \tan^{-1}X_s\right) \right| \quad (3d)$$

radii of the stubs are an optional feature in this design since the structure is to be additively manufactured. Nevertheless, we choose to incorporate the corner radii, as other designers can use our specified dimensions for either additive and subtractive manufacturing of their own.

B. High-Precision CNC Milled Mixed-Inverter Diplexer

For the design of the diplexer structure, the two filtering branches were designed separately, but in accordance with either an all-admittance inverter or all-impedance inverter selection. Although these constraints were chosen arbitrarily, it allows for a more academic and investigative exercise when comparing and contrasting the diplexer's capabilities. The design procedure is similar to the one described in Section II.A, but now includes the use of equation (3) for the impedance inverter schemes that are shown in Fig. 6. The first branch has been selected for the lower passband of the diplexer as an all-admittance inverter design that utilizes both E-plane and H-plane stubs and follows from equations (1) and (2). The second branch has been selected for the upper passband of the diplexer as an all-impedance inverter design that utilizes all H-plane irises and follows from equations (2) and (3). The lower and upper passbands have been designated for approximately 5 GHz bandwidth each; these passbands are defined from 95 GHz to 100 GHz, and 103 GHz to 108 GHz,

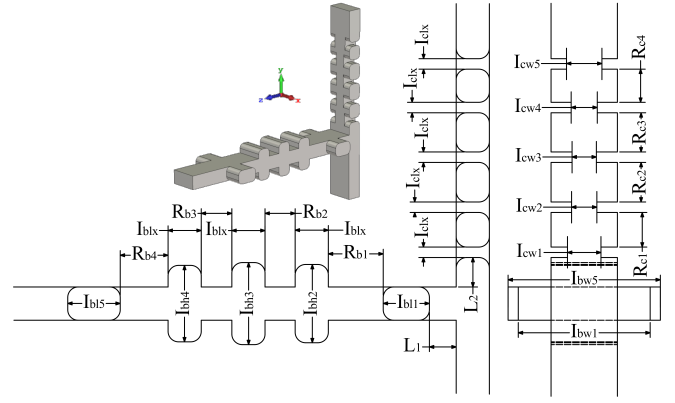


Fig. 7. Perspective view of the mixed-inverter diplexer's vacuum shell and its corresponding dimensions. Admittance inverter branch values: $R_{b1} = 2.102$ mm, $R_{b2} = 1.154$ mm, $R_{b3} = 1.172$ mm, $R_{b4} = 1.832$ mm, $I_{b1} = 1.768$ mm, $I_{bw1} = 5.050$ mm, $I_{bh2} = 2.990$ mm, $I_{bh3} = 3.134$ mm, $I_{bh4} = 2.920$ mm, $I_{blx} = 1.270$ mm, $I_{bl5} = 2.010$ mm, $I_{bw5} = 5.830$ mm, $L_1 = 1.026$ mm, and impedance inverter branch values: $R_{c1} = 1.321$ mm, $R_{c2} = 1.511$ mm, $R_{c3} = 1.496$ mm, $R_{c4} = 1.266$ mm, $I_{cw1} = 1.282$ mm, $I_{cw2} = 0.968$ mm, $I_{cw3} = 0.930$ mm, $I_{cw4} = 1.000$ mm, $I_{cw5} = 1.356$ mm, $I_{clx} = 0.400$ mm, $L_2 = 1.125$ mm.

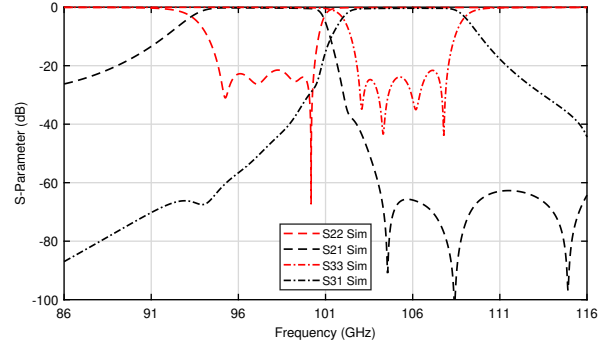


Fig. 8. S-parameters of the simulated mixed-inverter diplexer (conductivity of brass taken as 1.59×10^7 S/m).

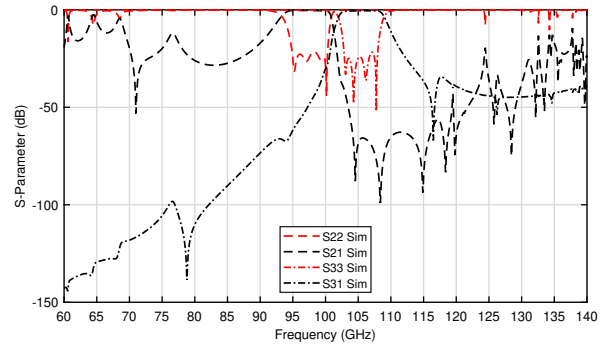


Fig. 9. Wide-band spurious performance of the simulated mixed-inverter diplexer (conductivity of brass taken as 1.59×10^7 S/m).

respectively. Synthesis based on the CIET is used for the initial design of each branch before final optimization as a mixed-inverter diplexer unit. Fig. 7 depicts a perspective view of the diplexer's vacuum shell and its corresponding dimensions. Fig. 8 exhibits the simulated S-parameters over the range of

86 GHz to 116 GHz. The upper passband takes the form of a standard Chebyshev filter, while the lower passband exhibits dispersive transmission zeros above its passband, which are typical of over-moded inverter stubs [10]. However, this can be advantageous in a diplexing format as shown in this example, since transmission zeros can be allocated without the need of cross-coupling or complex multi-mode designs and simultaneously avoid reduced waveguide height/width requirements that are typically used in advanced diplexing formats, for example: [17]–[24]. Fig. 9 demonstrates the wide-band spurious performance of the diplexer over the range of 60 GHz to 140 GHz, again beyond the definition of the W-band.

III. FABRICATION AND MEASUREMENT

For the fabrication of the filter, an *Elegoo Mars 2 MSLA* 3D-printer was selected for its nature as a low-cost hobbyist-type tool. The prototype is printed as two separate blocks along the E-plane with a 0.02 mm print layer height of non-conductive photo-polymer resin. As mentioned in the previous section, a radius of 0.3 mm has been added to the inverter stubs. At this stage in other filter works of this frequency range, an electroless plating method is used to uniformly coat the surfaces of the structure with a nickel-based seed layer for electroplating [3]–[5]. However, by printing the structure in an E-plane format, a low-cost copper-based aerosol spray [25] can be applied to each half of the filter blocks as a precursor, forgoing the need for chemical seed-baths, paint-gun spraying equipment, the design of specialized metallization slots for the component's interior structures, or professional printing and metallization services.

In general, copper electroplating is a rather coarse but simple method for plating plastic-based 3D-printed parts, especially when considering the micro-fine detail required for components at very high frequencies. Additionally, factors such as the enlargement and shrinkage of the component after photo-polymer resin curing must be accounted for in the fabrication process; these factors become highly critical in millimetre-wave design and must be suitably addressed. For the design at hand, it was found that non-uniform scaling factors were required for each of the coordinate directions of the internal filter dimensions. Using the x-y-z coordinates that have been defined in Fig. 3, the scaling factors which have lead to the reported results are 1.07% along the x-axis, 1.12% along the y-axis, and 1.00% along the z-axis. These scaling factors were determined through trial-and-error and are applied to the SLA-printed structure in order to balance the enlargement and shrinkage associated with curing of photo-polymer resin, the copper spray coating, and the final electroplating layer. The following outlines the general fabrication process, while Fig. 10(a) depicts the progression of the filter at several different stages of fabrication:

- 1) *3D Printing of the structure*; for the case at hand, an *Elegoo Mars 2 MSLA* 3D-printer has been selected for low-cost SLA printing with a print-layer height of 0.02 mm. After the structure is printed, it is cleaned with

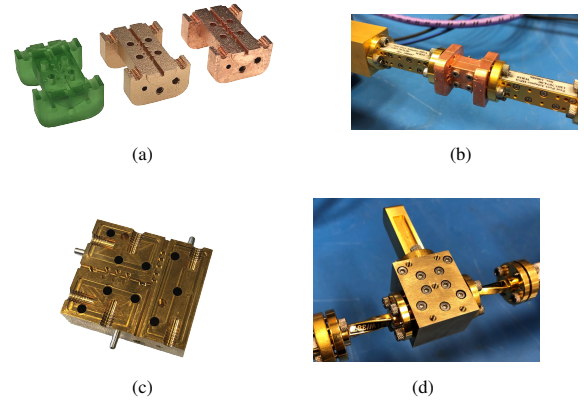


Fig. 10. Fabrication and assembly: a). Progression of the fabricated admittance-inverter filter; one half of the split-block is shown at different stages with respect the steps outlined in Section III: *3D-printing of the structure* (left), *post-printing stage 2*; copper spray coated (center), and after the *galvanization process*; with sufficient metallization (right), b). the assembled admittance-inverter filter connected to the test-bed, c). one half of the mixed-inverter diplexer after milling (shown along the E-plane), and d). the assembled mixed-inverter diplexer connected to the test-bed.

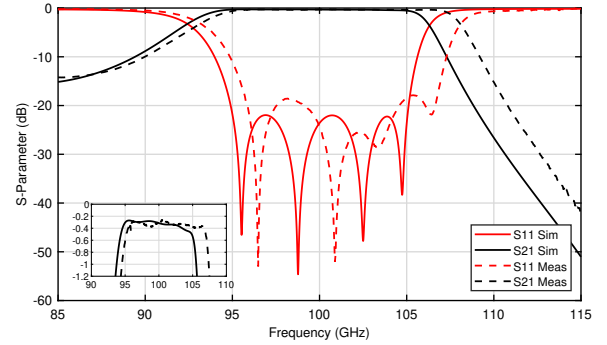


Fig. 11. Simulated versus measured S-parameters of the 3D-printed admittance-inverter filter. The inset shows a close up view of the insertion loss (equivalent conductivity of copper taken as 4.2×10^6 S/m).

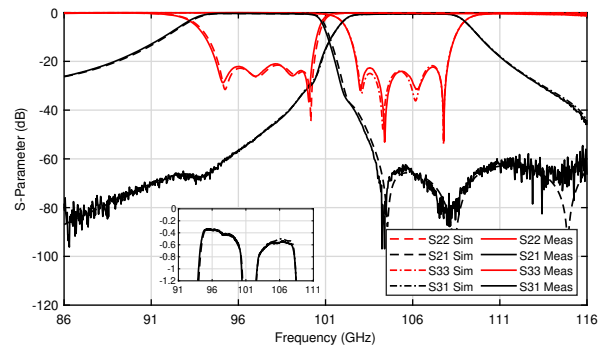


Fig. 12. Simulated versus measured S-parameters of the high-precision milled mixed-inverter diplexer. The inset shows a close up view of the insertion loss in the lower and upper passbands. (equivalent conductivity of brass taken as 7.7×10^6 S/m).

isopropyl alcohol to remove excess resin and then cured for 8 minutes in U.V. light.

- 2) *Post Printing Stage 1*; the threads of the flange holes

TABLE I.
Comparison of W-Band SLA-Fabricated Bandpass Filters†

f_c (GHz)	FBW	Insertion loss (dB)	Return loss (dB)	Commercial grade 3D-printing	Metallization technique	Construction profile	Reference
87.5	11.5%	0.3 - 0.5	>18	Yes	Ni Electroless & Cu/Au Electroplating	Mono-block	[4]
102.5	3.6%	1.0 - 2.0	<10	Yes	Ni Electroless & Cu Electroplating	Mono-block	[5]
107.2	6.34%	0.95*	>11	Yes	Ni Electroless & Cu Electroplating	Split-block	[3]
101.14	11.10%	0.26 - 0.48	>17	No	Cu aerosol spray & Cu Electroplating	Split-block	This work

TABLE II.
Comparison of W-Band CNC-based Fabricated Diplexers†

f_c (GHz)	FBW	Insertion loss (dB)	Return loss (dB)	Design type	Component parts	Reference
95.5 / 106.5	11.52% / 10.33%	1.5 / 1.7*	NA**	Substrate based fin-line	3	[26]
87.5 / 102.5	5.71% / 4.89%	1.0 / 1.0*	>10	Substrate based fin-line	3	[27]
90.0 / 110.0	11.11% / 9.09%	1.0 / 1.0*	>12	Substrate based fin-line	3	[27]
97.5 / 105.4	5.62% / 4.99%	0.34 - 0.76 / 0.55 - 0.88	>21	Direct coupled mixed inverter	2 (Split-block)	This work

†Table values are estimated as best as possible for the presented measured data where not directly reported. *Measured data was reported as the achieved typical values or at center frequency (rather than a range), **Data not available.

are threaded by hand and the structure is cleaned with galvano-degreaser and distilled water and then left to air dry.

- 3) *Post Printing Stage 2*; primary and secondary layers of copper aerosol spray are applied for approximately 1 - 2 seconds for each pass until all of the resin is coated. The sprayed coating is left to dry for 12 hours.
- 4) *Galvanization Process*; electroplating is conducted in acidic copper electrolyte for 2 hours at 400 mA with a distance of 85 mm from the cathode. After removal, the structure is cleaned with distilled water, dried, and the flange threads are re-tapped to clean out excess copper and debris.
- 5) *Quality Control*; mechanical (caliper) and electrical (VNA) measurements are made to test the structure. Poor metallization or measurements require the vacuum structure and/or housing to be scaled accordingly. The process is reiterated from Step 1 until the desired specifications are met.

Upon reaching the *Quality Control* stage of the fabrication process outlined above, the two filter halves are fastened together by mounting-screws through each half of the component body (as shown in Fig.10(b)). The pliability and the fine surface finish of the 3D-printed part allows for the two halves to be compressed adequately and allows for any localized air gaps to be mitigated. Measurement of the filter allows for errors to be identified and corrected in an iterative fabrication process. For example; a deviation in measured center frequency can require a re-scaling of the filter dimensions, or conversely, poor

measured insertion loss can require a thicker metallization layer, where the electroplating duration and current can be adjusted and the structure re-scaled accordingly. Iterations can be made to adjust the process until the desired response is met.

A comparison of the simulated and measured results over the range of 85 GHz to 115 GHz is presented in Fig. 11 while Fig. 10(b) depicts the filter connected to the test-bed. This comparison demonstrates good measured results; the measured return loss is better than 17 dB throughout the passband, and the measured insertion loss is on the range of 0.26 dB to 0.48 dB, ultimately, demonstrating that a very coarse method of fabrication and metallization can be applied to achieve good results when compared to other W-band SLA-printed designs that utilize more professional or commercial-based methods [3]–[5]. The measured surface roughness (S_a) is found to be approximately 3 μm , where S_a describes the mean arithmetic height. In regards to the deviation between the simulated and measured results, this difference can be attributed to several factors such as small misalignments, sub-optimal dimensional scaling and non-uniform metallization thicknesses. However, as discussed previously, more iterations can be applied during the fabrication process in order to reach the optimal desired performance and further reduce the shift in measured center frequency.

For the fabrication of the diplexer, brass has been selected as the cutting material due to its machinability and final surface finish. The prototype is split into two separate blocks along the E-plane for high-precision CNC milling. The E-plane has been selected as the optimal cutting plane as it is known to

minimize disturbances of the surface current distribution as well as reduce passive intermodulation (PIM) effects in high-power applications [19]. The milling radius for both of the diplexer branches has been set to 0.4 mm. Fig. 10(c) and 10(d) depict the internally milled structures of the diplexer and the fully assembled unit connected to the test-bed. No silver or gold coating has been applied to the structure. The measured surface roughness S_a is found to be approximately 1 μm .

A comparison of the simulated and measured results of the diplexer are presented in Fig. 12 over 86 GHz to 116 GHz. This comparison demonstrates good measured results in both of the passbands. The measured return loss is better than 21 dB throughout both the lower and upper passbands while the measured insertion losses are on the range of 0.34 dB to 0.76 dB and 0.55 dB to 0.88 dB for the lower and upper passbands, respectively. Although the passbands are slightly different in respect to final bandwidth and center frequency, they are still relatively similar enough to note that for both the simulated and measured results, the admittance inverter branch exhibits a slightly better insertion loss value when compared to the impedance inverter branch. This difference in insertion loss is approximately 0.14 dB when comparing the measured center frequencies of 97.5 GHz and 105.4 GHz, and is highlighted in the inset of Fig. 12 over a range of 91 GHz to 111 GHz.

IV. LITERATURE COMPARISON

For both the filter and the diplexer, a comparison is made to fabricated W-band prototypes of the same technologies in the current literature. Although there are few to be compared at this time, an attempt is made to make a direct comparison between the key differences in fabrication style and measured results for WR-10 profiles. Table I highlights the existing W-band SLA-printed filters, while Table II highlights the existing W-band CNC-based filters. In both cases, competitive results can be observed; for the SLA filter, a low insertion loss has been achieved using low-cost printing and metallization techniques, while the high-precision milled diplexer exhibits low insertion losses in a unique split-block profile. Furthermore, the filter and the lower-passband branch of the diplexer remain free of any intersection of the base waveguide dimensions.

V. CONCLUSION

The first instances of a 3D-printed filter and high-precision CNC milled diplexer that utilize arbitrary inverter sequences is reported for operation in the W-band. Examination of the models demonstrate the use of admittance inverters and their potential use in future millimetre and sub-millimetre wave frequencies. The filter which has been presented, has for the first time been fabricated using a low-cost and coarse method to demonstrate the use of a hobbyist 3D-printing and metallization technique in order to reach the 100 GHz region, while the diplexer which has been presented, has been fabricated using high-precision CNC milling in order to demonstrate a unique design profile that contrasts the subtle differences between all-admittance and all-impedance inverter models. This work depicts two of the few instances of arbitrary

inverter sequences for waveguide design in the literature and exhibits their potential use for overcoming fabrication challenges in micro-scale designs. Future exploration of this topic can aim to include many new designs for overcoming size constraints, difficult fabrication profiles, multipaction, and stringent responses, as well as promote low-cost research options for academic and commercial enterprises.

REFERENCES

- [1] R. Prasad, *5G Outlook - Innovations and Applications*. Delft, The Netherlands: River Publishers, 2016.
- [2] Y. Balal and Y. Pinhasi, "Atmospheric effects on millimeter and sub-millimeter (THz) satellite communication paths," *J. Infr. Millim. and Terah. Waves*, vol. 40, no. 2, pp. 219–230, 2019.
- [3] M. D'Auria, W. J. Otter, J. Hazell, B. T. Gillatt, C. Long-Collins, N. M. Ridler, and S. Lucyszyn, "3-D printed metal-pipe rectangular waveguides," *IEEE Trans. Compon. Packag. Manuf. Technol.*, vol. 5, no. 9, pp. 1339–1349, 2015.
- [4] X. Shang, P. Penchev, C. Guo, M. J. Lancaster, S. Dimov, Y. Dong, M. Favre, M. Billod, and E. De Rijk, "W-band waveguide filters fabricated by laser micromachining and 3-D printing," *IEEE Trans. Microw. Theory Tech.*, vol. 64, no. 8, pp. 2572–2580, 2016.
- [5] C. Guo, J. Li, X. Shang, M. J. Lancaster, J. Xu, X. He, Y. Gao, and X.-Y. Zhai, "Novel microwave/millimeter-wave passive waveguide devices based on 3-D printing techniques," *J. Infr. Millim. Waves*, vol. 36, no. 1, pp. 81–91, 2017.
- [6] B. Zhang and H. Zirath, "3D printed iris bandpass filters for millimetre-wave applications," *IET Electron. Lett.*, vol. 51, no. 22, pp. 1791–1793, 2015.
- [7] K. Fujiwara, R. Kobayashi, S. Kuwahara, S. Takemura, K. Takizawa, and Y. Watanabe, "3-D printed iris waveguide filter in W-band," in *23rd Int. Microw. and Radar Conf. (MIKON)*, Warsaw, Poland, Oct. 2020, pp. 346–349.
- [8] M. Salek, X. Shang, R. C. Roberts, M. J. Lancaster, F. Boettcher, D. Weber, and T. Starke, "W-band waveguide bandpass filters fabricated by micro laser sintering," *IEEE Trans. Circuits Syst., II, Exp. Briefs*, vol. 66, no. 1, pp. 61–65, 2018.
- [9] M. Salek, X. Shang, M. J. Lancaster, R. C. Roberts, T. Starke, F. Boettcher, and D. Weber, "90 GHz micro laser sintered filter: Reproducibility and quality assessment," in *49th Eur. Microw. Conf. (EuMC)*, Paris, France, Oct. 2019, pp. 296–299.
- [10] Q. Wang and J. Bornemann, "Synthesis and design of direct-coupled rectangular waveguide filters with arbitrary inverter sequence," in *Proc. 16th Int. Symp. Antenna Tech. Appl. Electromagn. (ANTEM)*. Victoria, Canada: IEEE, Jul. 2014, pp. 1–6.
- [11] J. Uher, J. Bornemann, and U. Rosenberg, *Waveguide components for antenna feed systems: Theory and CAD*. Artech House Antenna Library, 1993.
- [12] S. Amari, J. Bornemann, and R. Vahldieck, "Accurate analysis of scattering from multiple waveguide discontinuities using the coupled-integral equations technique," *J. Electromagn. waves and applicat.*, vol. 10, no. 12, pp. 1623–1644, 1996.
- [13] —, "Fast and accurate analysis of waveguide filters by the coupled-integral-equations technique," *IEEE Trans. Microw. Theory Tech.*, vol. 45, no. 9, pp. 1611–1618, 1997.
- [14] J. Bornemann, U. Rosenberg, S. Amari, and R. Vahldieck, "Edge-conditioned vector basis functions for the analysis and optimization of rectangular waveguide dual-mode filters," in *IEEE MTT-S Int. Microw. Symp. Dig. (IMS)*, vol. 4, Anaheim, USA, Jun. 1999, pp. 1695–1698.
- [15] G. L. Matthaei, L. Young, and E. M. T. Jones, *Microwave filters, impedance-matching networks, and coupling structures*. Artech house, 1980.
- [16] S. Zhang and L. Zhu, "Synthesis method for even-order symmetrical chebyshev bandpass filters with alternative J/K inverters and $\lambda/4$ resonators," *IEEE Trans. Microw. Theory Tech.*, vol. 61, no. 2, pp. 808–816, 2012.
- [17] W. Menzel, F. Alessandri, A. Plattner, and J. Bornemann, "Planar integrated waveguide diplexer for low-loss millimeter-wave applications," in *1997 27th European Microwave Conference*, Jerusalem, Israel, Sep. 1997, pp. 676–680.

- [18] S. Amari, J. Bornemann, W. Menzel, and F. Alessandri, "Diplexer design using pre-synthesized waveguide filters with strongly dispersive inverters," in *IEEE MTT-S Int. Microw. Symp. Dig. (IMS)*, Phoenix, USA, May. 2001, pp. 1627–1630.
- [19] S. H. Yun, M. S. Uhm, and I. B. Yom, "Design of the multipaction free high power Ka-band diplexer with an E-plane T-junction," in *Asia-Pacific Conf. Commun.* IEEE, 2005, pp. 582–585.
- [20] F. Teberio, I. Arregui, M. Guglielmi, A. Gomez-Torrent, P. Soto, M. Laso, and V. Boria, "Compact broadband waveguide diplexer for satellite applications," in *IEEE MTT-S Int. Microw. Symp. Dig.*, San Francisco, USA, May. 2016, pp. 1–4.
- [21] F. Teberio, I. Arregui, P. Soto, M. A. Laso, V. E. Boria, and M. Guglielmi, "High-performance compact diplexers for Ku/K-band satellite applications," *IEEE Trans. Microw. Theory Tech.*, vol. 65, no. 10, pp. 3866–3876, 2017.
- [22] U. Rosenberg, A. Bradt, M. Perelshtein, and P. Bourbonnais, "Extreme broadband waveguide diplexer design for high performance antenna feed systems," in *Proc. Eur. Microw. Conf. (EuMC)*, Paris, France, Sep. 2010, pp. 1249–1252.
- [23] J. R. Aitken and J. Hong, "Design of millimetre wave diplexers with relaxed fabrication tolerances," *IET Microw., Antennas & Propag.*, vol. 9, no. 8, pp. 802–807, 2015.
- [24] H. Setti, A. Tribak, A. El Hamichi, L. Yechou, and A. Mediavilla, "Design and manufacture of a diplexer for K/Ka band satellite applications," *Int. J. of Sci. and Eng. Resear.*, vol. 9, no. 10, pp. 914–918, 2018.
- [25] "Tifoo shop. [online]." Available: <https://www.tifoo.de/>, accessed: 13-Apr-2021.
- [26] C. Nguyen and K. Chang, "Design and performance of a W-band broadband finline diplexer with over 20 GHz bandwidth," in *IEEE MTT-S Int. Microw. Symp. Dig. (IMS)*, St. Louis, USA, Jun. 1985, pp. 349–352.
- [27] Y.-C. Shih, L. Q. Bui, and T. Itoh, "Millimeter-wave diplexers with printed circuit elements," *IEEE Trans. Microw. Theory Tech.*, vol. 33, no. 12, pp. 1465–1469, 1985.



Chad Bartlett (Student Member, IEEE) was born in Nelson, BC, Canada in 1987. He received his B.Eng and M.Eng in Electrical Engineering from the University of Victoria in 2017 and 2019, respectively. He is currently pursuing a Dr.-Ing. degree at the Chair of Microwave Engineering, Institute of Electrical Engineering and Information Engineering, University of Kiel, Kiel, Germany. and is a member of the European Union's Horizon 2020 research and innovation programme for early-stage researchers.

His primary research interests include microwave and millimeter-wave passive components, filters and antenna networks for the next generation of satellite and communication systems, as well as developing methods for overcoming challenges in micro-scale designs.



Jens Bornemann (Life Fellow, IEEE) received the Dipl.-Ing. and the Dr.-Ing. degrees, both in electrical engineering, from the University of Bremen, Germany, in 1980 and 1984, respectively. From 1984 to 1985, he worked as an engineering consultant. In 1985, he joined the University of Bremen, Germany, as an Assistant Professor. Since April 1988, he has been with the Department of Electrical and Computer Engineering, University of Victoria, Victoria, B.C., Canada, where he became a Professor in 1992. From 1992 to 1995, he was a Fellow of the British

Columbia Advanced Systems Institute. In 1996, he was a Visiting Scientist at Spar Aerospace Limited (now MDA Space), Ste-Anne-de-Bellevue, Québec, Canada, and a Visiting Professor at the Microwave Department, University of Ulm, Germany. From 1997 to 2002, he was a co-director of the Center for Advanced Materials and Related Technology (CAMTEC), University of Victoria. From 1999 to 2002, he served as an Associate Editor of the IEEE Transactions on Microwave Theory and Techniques in the area of Microwave Modeling and CAD. From 2006 to 2008, he was an Associate Editor of the International Journal of Electronics and Communications. In 2003, he was a Visiting Professor at the Laboratory for Electromagnetic Fields and Microwave Electronics, ETH Zurich, Switzerland. From 1999 to 2009, he served on the Technical Program Committee of the IEEE MTT-S International Microwave Symposium. He has coauthored Waveguide Components for Antenna Feed Systems - Theory and Design (Artech House, 1993) and has authored/coauthored more than 350 technical papers. His research activities include RF/wireless/ microwave/millimeter-wave components and systems design, and field-theory-based modeling of integrated circuits, feed networks and antennas.

Dr. Bornemann is a Registered Professional Engineer in the Province of British Columbia, Canada. He is a Fellow IEEE, a Fellow of the Canadian Academy of Engineering (CAE), a Fellow of the Engineering Institute of Canada (EIC) and serves on the editorial advisory board of the International Journal of Numerical Modelling.



Michael Höft (Senior Member, IEEE) was born in Lübeck, Germany, in 1972. He received the Dipl.-Ing. degree in electrical engineering and the Dr.-Ing. degree from the Hamburg University of Technology, Hamburg, Germany, in 1997 and 2002, respectively. From 2002 to 2013, he joined the Communications Laboratory, European Technology Center, Panasonic Industrial Devices Europe GmbH, Lüneburg. He was a Research Engineer and then the Team Leader, where he had been engaged in research and development of microwave circuitry and components,

particularly filters for cellular radio communications. From 2010 to 2013, he was the Group Leader of research and development of sensor and network devices. Since October 2013, he has been a Full Professor with the Faculty of Engineering, University of Kiel, Kiel, Germany, where he is currently the Head of the Microwave Group, Institute of Electrical and Information Engineering. His research interests include active and passive microwave components, submillimeter-wave quasioptical techniques and circuitry, microwave and field measurement techniques, microwave filters, microwave sensors, and magnetic field sensors. Dr. Höft is a member of the European Microwave Association (EuMA), the Association of German Engineers (VDI), and the German Institute of Electrical Engineers (VDE).